UNIVERSIDAD REGIONAL AMAZÓNICA IKIAM

Facultad de Ciencias de la Tierra y Agua

Ingeniería en Geociencias

Estudio de la cámara magmática principal del volcán Sumaco mediante tomografía sísmica

Anderson Isaac Guamán Viveros

09 de diciembre de 2020, ciudad de Tena, Napo, Ecuador.

Declaración de derecho de autor, autenticidad y responsabilidad

Tena, 09 de diciembre de 2020

Yo, Anderson Isaac Guamán Viveros con documento de identidad N° 1004008106, declaro que los resultados obtenidos en la investigación que presento en este documento final, previo a la obtención del título de Ingeniero en Geociencias son absolutamente inéditos, originales, auténticos y personales.
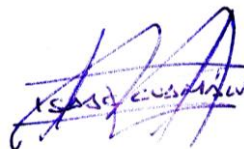
En virtud de lo cual, el contenido, criterios, opiniones, resultados, análisis, interpretaciones, conclusiones, recomendaciones y todos los demás aspectos vertidos en la presente investigación son de mi autoría y de mi absoluta responsabilidad.

Por la favorable atención a la presente, suscribo de usted,

Atentamente,

Firma:

_____

Anderson Isaac Guamán Viveros

Certificado de dirección de trabajo de integración curricular

Certifico que el trabajo de integración curricular titulado: "Estudio de la cámara magmática principal del volcán Sumaco mediante tomografía sísmica", en la modalidad de: proyecto de investigación en formato artículo original, fue realizado por: Anderson Isaac Guamán Viveros, bajo mi dirección.

El mismo ha sido revisado en su totalidad y analizado por la herramienta de verificación de similitud de contenido; por lo tanto, cumple con los requisitos teóricos, científicos, técnicos, metodológicos y legales establecidos por la Universidad Regional Amazónica Ikiam, para su entrega y defensa.

Tena, 29 de octubre de 2020

Firma:

....

José Sebastián Araujo Soria, PhD.

C.I: 1802672871

Solicitud para la designación del tribunal de grado
del trabajo de integración curricular

Tena, 09 de diciembre de 2020

Señor
Decano de la Facultad de Ciencias de la Tierra y Agua
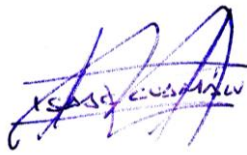Su despacho.

De mi consideración:

De conformidad con el Art. 12, literal 3, del Reglamento de Titulación de la Universidad Regional Amazónica Ikiam, yo, Anderson Isaac Guamán Viveros con documento de identidad N° 1004008106, estudiante de la carrera de Ingeniería en Geociencias, solicito a usted muy comedidamente, se designe el tribunal de grado para la revisión y calificación del trabajo de integración curricular, titulado "Estudio de la cámara magmática principal del volcán Sumaco mediante tomografía sísmica", en la modalidad de: proyecto de investigación en formato artículo original (Art. 11. Reglamento de Titulación de Ikiam).

Por la atención prestada, le anticipo mi agradecimiento.

iv

Atentamente,

Firma:

_____

Teléfono: 0992584125
Mail: anderson.guaman@est.ikiam.edu.ec

Adjuntos:
- Un ejemplar en digital del trabajo de integración curricular.
- Anexo 1. Declaración de derecho de autor, autenticidad y responsabilidad
- Anexo 2. Certificado de dirección de trabajo de integración curricular
- Fotocopia de la resolución de aprobación de prórroga (de ser el caso)
- Carta del tutor sugiriendo 3 posibles miembros del tribunal del grado (optativo)

INVESTIGACIÓN | Parroquia Muyuna, kilómetro 7 vía a Alto Tena
INNOVACIÓN | Tena · Napo · Ecuador
EDUCACIÓN | Telf.: (06) 370 0040 · (06) 299 9160

www.ikiam.edu.ec
@u_ikiam   IkiamOficial   u_ikiam   Universidad Ikiam

ESPACIO RESERVADO PARA UNIDAD DE INTEGRACIÓN CURRICULAR DE LA FACULTAD DE
_____

Conforme al Art. 12, literal 4, la Unidad de Integración Curricular en su sesión ordinaria _____ de fecha _____ designa a los siguientes profesores como miembros del Tribunal de Grado:

Miembro 1: _____.

Miembro 2: _____.

Miembro 3: _____.

Firma de los miembros de la Unidad de Integración Curricular:

_____

Decano/a:
Fecha:

_____

Director/(a) de carrera:
Fecha:

v _____

_____

Director/(a) de carrera:
Fecha:

_____

Profesor/a:
Fecha:

_____

Profesor/a:
Fecha:

INVESTIGACIÓN | Parroquia Muyuna, kilómetro 7 vía a Alto Tena
INNOVACIÓN | Tena · Napo · Ecuador
EDUCACIÓN | **Telf.:** (06) 370 0040 · (06) 299 9160

www.ikiam.edu.ec
@u_ikiam   IkiamOficial   u_ikiam   Universidad Ikiam

AGRADECIMIENTOS

ÍNDICE GENERAL

ÍNDICE DE FIGURAS

RESUMEN

El arco posterior (cinturón subandino oriental) de los Andes ecuatorianos comprende cuatro volcanes: El Reventador, Yanaurco, Pan de Azúcar y Sumaco. A pesar de la proximidad de estos volcanes, los materiales volcánicos del Sumaco son claramente alcalinos insaturados en SiO_2. Mediante tomografía sísmica de tiempo de viaje, se generaron tres modelos de velocidad (v_P, Δv_P, v_P/v_S) para identificar el reservorio magmático principal del arco posterior ecuatoriano.

El problema inverso se resolvió utilizando el paquete de códigos informáticos INSIGHT en una caja paralelepípeda cuadriculada con un tamaño de celda de 5 km en dirección horizontal y 2 km en dirección vertical. Este estudio determina la cámara magmática principal ubicada debajo del volcán Sumaco pero ligeramente compartida con los volcanes extintos Pan de Azúcar y Yanaurco.

La extensión de la falla Sumaco también es reconocible, la cual se espera que sea responsable del rápido ascenso del magma hacia la superficie antes de un evento eruptivo.

Una conclusión importante de esta investigación es que un factor significativo que podría conducir a la diferenciación de las lavas de Sumaco es la subducción hipotética de una sección plana de la corteza oceánica debajo del volcán.

Palabras clave: Andes, cinturón Subandino Oriental, volcán Sumaco, tomografía sísmica, cámara magmática.

INVESTIGACIÓN | Parroquia Muyuna, kilómetro 7 vía a Alto Tena
INNOVACIÓN | Tena · Napo · Ecuador
EDUCACIÓN | Telf.: (06) 370 0040 · (06) 299 9160

www.ikiam.edu.ec
@u_ikiam   IkiamOficial   u_ikiam   Universidad Ikiam

ABSTRACT

The back-arc (Eastern sub-Andean belt) of the Ecuadorian Andes encompass four volcanoes: Reventador, Yanaurco, Pan de Azúcar, and Sumaco. Despite the proximity of these volcanoes, Sumaco volcanic materials are distinctly SiO_2-undersaturated alkalines. Through seismic travel time tomography, three velocity models (v_P, Δv_P, v_P/v_S) were generated to identify the primary magmatic reservoir of the Ecuadorian back-arc. The inverse problem was solved using the INSIGHT computer code package in a gridded parallelepiped box with a cell size of 5 km in the horizontal direction and 2 km in the vertical direction. This study finds the principal magmatic chamber located below the Sumaco volcano but slightly shared with the extinct Pan de Azúcar and Yanaurco volcanoes.

Sumaco Fault extension is also recognizable and is expected to be responsible for the rapid ascent of the magma towards the surface before an eruption.

x

As a conclusion, a significant factor that could lead to the differentiation of the Sumaco lavas is a hypothetical flat slab block below the volcano.

Keywords: Andes, Eastern sub-Andean belt, Sumaco volcano, seismic tomography, magmatic chamber.

INVESTIGACIÓN | Parroquia Muyuna, kilómetro 7 vía a Alto Tena
INNOVACIÓN | Tena · Napo · Ecuador
EDUCACIÓN | **Telf.:** (06) 370 0040 · (06) 299 9160

www.ikiam.edu.ec

@u_ikiam   IkiamOficial   u_ikiam   Universidad Ikiam

Study of the primary magmatic chamber of the Sumaco volcano by seismic tomography

INTRODUCTION

Since the mid-1970s, seismic tomography has been a widely used geophysical technique that has had a great impact on solid-Earth sciences by answering some basic questions of geodynamics (Zhao, 2015). Starting from arrival times of body waves recorded by seismometers, seismic travel time tomography attempt to describe, deduce or infer the internal structure of the Earth at a variety of scales through the seismic velocity models determination (Nolet, 2008).

This technique has proved to obtain unprecedented clear images in zones of high seismicity levels and regions with dense coverage of seismic stations. Accurate reconstructed images of the subducting slab, mantle anomalies, and magma chambers can be achieved by seismic travel time tomography in different types of tectonic setting (e.g., Zhou and Clayton, 1990; Rowan and Clayton, 1993; Spakman et al., 1993; McNamara et al., 1997; Sekiguchi, 2001; Husen et al., 2004; Li and van der Hilst, 2010; Paulatto et al., 2012).

The abundant seismic data recorded in Ecuador due to the eastward subduction of both the oceanic Nazca plate and the aseismic Carnegie Ridge beneath the South America continental plate (Figure 1) represents an outstanding potential to resolve seismic travel time tomography and thus improve the comprehension of their peculiar subduction-related volcanic arc system. Nevertheless, to date, there are few seismological research about this subject in Ecuador

either with a volcanic (Molina et al., 2005; Garcia-Aristizabal et al., 2007) or regional (Prevott et al., 1996; Gailler et al., 2007; Araujo, 2016; Lynner et al., 2020) approach.

In the northern half of the Ecuadorian Andes, 55 Quaternary volcanoes are distributed in three sub-parallel mountain ranges: the frontal arc (Western Cordillera), the main arc (Real Cordillera) and the back-arc (Eastern sub-Andean belt). Across this wide magmatic arc, volcanoes show substantial lateral geochemical variation (Barragan et al., 1998; Bryant et al., 2006; Chiaradia et al., 2009; Hidalgo et al., 2012; Chiaradia et al., 2014).

The Reventador, Yanaurco, Pan de Azúcar, and Sumaco are the last southern volcanoes of the Northern Volcanic Zone (NVZ) over the back-arc in Ecuador. However, despite the proximity of these volcanoes, Sumaco geochemical composition is different, even among the other volcanoes of Ecuador. Volcanic materials of Sumaco are distinctly SiO_2-undersaturated alkaline and show absarokitic to shoshonitic affinity, whereas the rest of Ecuadorian volcanoes produce medium to high-K calc-alkaline lavas (Barragan et al., 1998; Chiaradia et al., 2009). The alkalinity of the Sumaco lavas is considerably higher than other typical continental back-arc products such as Kamchatka (Volynets et al., 2010; Garrison et al., 2018).

This study reports the lithosphere velocity models beneath the Sumaco volcano obtained from tomographic inversion of travel time data. This paper aims to identify the three-dimensional arrangement of the slab beneath the Sumaco volcano and infer how this influences their main magmatic reservoir and geochemical composition. The resulting tomographic images are consistent with previous geochemical and petrographic models of the Sumaco lavas and shed new light on understanding the volcanic arc in Ecuador.

Geological setting and geochemistry

The Ecuadorian sub-Andean zone (or back-arc) is the easternmost compressional belt between the Cordillera Real and the Amazonian basin and is characterized by erosive processes and landslides (e.g., Bes de Berc, 2003; Laraque et al., 2009), and both intense seismic and volcanic activity (e.g., Legrand et al., 2005; Lees et al., 2008). In their outcrops of folded strata, it is possible to recognize steep west-dipping reverse faults with N-S to NNE-SSW orientation, which shows a dextral behavior (Ham and Herrera, 1963; Balkwill et al., 1995).

The sub-Andean zone, which has sustained an uplift and deformation mainly during the Middle-Late Miocene to Early Quaternary (Ruiz, 2002), comprises three morpho-tectonic units from north to south: (1) the Napo Uplift, (2) the Pastaza Depression, and (3) the Cutucú Cordillera.

The Napo Uplift is a large anticline dome limited by faults in its west and east edges. It is composed of a granitic batholith (Abitagua) in the west and compression structures such as positive flower structures to the east, together with Cretaceous-Tertiary sedimentary facies outcrops (Baby et al., 1998).

The Sumaco volcano (0.54º S, 77.63º W) is located in the south of the Napo Uplift (Figure 2). This is the easternmost active volcano of the Ecuadorian magmatic arc located ~400 km from the trench and is built upon ~40 km thick continental crust (Araujo, 2016) over the Jurassic-Cretaceous sedimentary sequence that overlies South American Precambrian craton (Dashwood and Abbotts, 1990; Chiaradia et al., 2009).

There are reports of at least three possible explosive eruptions of Sumaco volcano (Siebert et al., 2011) with Strombolian to Vulcanian eruption types (Barragán and Baby, 2004). A study of the Sumaco's recent volcanic deposits shows a reduced volcanic activity (Volcanic Explosivity Index VEI=3 to 4) during the last 360±30 last years with a roughly estimated recurrence rate of ~60 years (Salgado, 2019). Based on reports of their summit crater morphology is probable that the most recent volcanic event occurred in 1933 (Hall, 1997; Siebert et al., 2011).

Sumaco is a stratovolcano with a basal diameter of approximately 20 km that rises 3990 m.a.s.l. This volcano has a dense plant cover up to an elevation of 3200 m. The diameter of their summit crater is ~100 m and includes slightly eroded remnants of both small lava domes and spatter cones structures from eruptions of unknown age (Garrison, 2018). The present-day Sumaco was built up during three volcanic phases, which are separated by two sliding scars: 1) Paleo Sumaco, 2) Recent Sumaco, and 3) Current Sumaco (Salgado, 2019).

Sumaco's lavas have a peculiar mineral assemblage and chemistry. These lavas have an alkaline geochemical composition with porphyritic textures characterized by phonolites, basanites, and feldspathoid-bearing tephrites rocks containing modal haüyne and normative nepheline (Barberi et al., 1988; Barragan et al., 1998). Phenocrystals of olivine, apatite, magnetite, nosean, leucite, sodium augite, clinopyroxene, and plagioclase are present in their mineral assemblage (Bourdon et al., 2003; Barragán and Baby 2004).

Sumaco's lavas major elements composition displays the highest content of K_2O, P_2O_5 and Na_2O and the lowest values of SiO_2 among the other Ecuadorian volcanoes which shows their absarokitic to shoshonitic affinity (Bryant et al., 2006; Garrison et al., 2018). Likewise, lavas of

Sumaco are strongly enriched in all incompatible elements and rare earth elements (Bourdon et al., 2003; Chiaradia et al., 2009).

THE DATA

The preprocessed data from Araujo, 2016, was used in this study. This data consists of arrival times of P and S waves, recorded in 4 different networks. These records come from the Red Nacional de Sismógrafos del Instituto Geofísico de la Escuela Politécnica Nacional del Ecuador (RENSIG), the Red Sísmica Nacional del Instituto Geofísico del Perú (RSN) and from two seismic experiments: Andes Du Nord (ADN) project and a temporary network installed in Northern Peru.

To merge these four datasets was necessary to harmonize the different observational errors to identify later the records corresponding to the same seismic event. The RENSIG catalog was considered as a reference scale to harmonize the observational uncertainties from these data sets.

The outliers derived from the P and S phase picking process were removed using a Wadati diagram (Wadati and Oki, 1933). The estimation of the v_P/v_S ratio from this diagram is 1.74. Based on the filtered data, the localization of the seismic events was performed with the HypRef code (Thouvenot and Fréchet, 2006). Those events located outside the inversion box and the events with less than 5 data or with less than 3 P phases were also removed.

The final data set or catalogue of events consists of 404,097 P phases and 167,245 S phases associated with 45,941 seismic events with magnitude greater than 2.5 ranging from 1988 to 2016.

METHODS OF STUDY

The Bayesian approach

The method used for this tomography study is based on a stochastic inversion (Tarantola and Valette, 1982), which leads to a Tikhonov regularization problem. The generic data and model vectors are denoted by $\mathbf{d} \in D$ and $\mathbf{m} \in M$ respectively, which are Gaussian with expectations $\mathbf{d}_{obs}$ and $\mathbf{m}_{prior}$ and with covariances $\mathbf{C}_d$ and $\mathbf{C}_m$. The catalogue data ($\mathbf{d}_{obs}$) requires to be complemented according to a hyperbolic secant probabilistic density function (Eq. 1) associated with the errors in the measurements of each data d to enhance the robustness in the inversion process.

$$\rho_{obs}(d) = \frac{1}{2\sigma_{obs}} \frac{1}{cosh\left(\frac{\pi}{2}\frac{d-d_{obs}}{\sigma_{obs}}\right)} \tag{1}$$

The generic model vector $\mathbf{m}=[\upsilon_P, \upsilon_P/\upsilon_S, \boldsymbol{x}, \boldsymbol{t}_0, \Delta^P, \Delta^{S-P}]$ contain the values of the P wave velocity (υ_P), the ratio between the P and S velocity (υ_P/υ_S), the hypocenter ($\boldsymbol{x}$) and the origin time ($\boldsymbol{t}_0$) of the seismic events, and the delay times attached to each station (Δ^P, Δ^{S-P}). The delay values account for possible local effects around the stations. The generic data vector $\mathbf{d}$ used as input corresponds to the P-waves arrival times ($\mathbf{d}^P = t_P$) and the differences between S and P waves arrival times ($\mathbf{d}^{S-P} = t_S - t_P$).

The model parameters to be identified in our study depend on the usual space (R^3), thus the model space M consists of square integrable scalar functions describing a physical quantity depending on the position. The theoretical mapping g that links the model vector $\mathbf{m}$ to the

data vector **d** is defined as Eq. (2), where the P-wave travel times (T_i^P) and the difference in travel times (ΔT_i) are denoted as Eq. (3) and (4) respectively:

$$d = \begin{bmatrix} d^{S-P} \\ d^P \end{bmatrix} = g(\boldsymbol{m}) = \begin{bmatrix} \Delta\,T_i\left(v_P, v_P/v_S, \boldsymbol{x}_{j(i)}\right) + \Delta_{k(i)}^{S-P} \\ T_i^P\left(v_P, \boldsymbol{x}_{j(i)}\right) + t_{0i} + \Delta_{k(i)}^P \end{bmatrix} \tag{2}$$

$$T_i^P = \int\limits_{\mathcal{R}_i^P} \frac{ds}{v_P(s)} \tag{3}$$

$$\Delta T_i = \int\limits_{\mathcal{R}_i^S} \frac{v_P}{v_S}(s)\frac{ds}{v_P(s)} - \int\limits_{\mathcal{R}_i^P} \frac{ds}{v_P(s)} \tag{4}$$

where s represent the curvilinear abscissa along the ray and $\mathcal{R}_i^P$ and $\mathcal{R}_i^S$ represent the ray pathway of the P and S waves from the hypocenter to the station.

The inverse problem of travel time tomography

According to the length of the study area, the GRS80 ellipsoid was chosen as a reference for the shape of the Earth. Additionally, the topography of the surface was included above this ellipsoid to provide more fidelity to the results.

To solve the inverse problem, a 1-D prior velocity model for the P-wave was settled as a function of the geographical depth. The increase of the velocity from the surface of the topography ($v_{surf} = 4$ km/s) to the surface of the ellipsoid ($v_0 = 4.5$ km/s) is defined by a linear increment. This velocity model is simply divided into three parts: the crust, the most upper part of the upper mantle and the rest of the mantle until it reaches 244 km of depth.

The a priori velocity model for the S-wave was obtained using the υ_P/υ_S ratio from the Wadati diagram. The Moho topography is not considered within these a priori velocity models.

Accurate prior localization of the seismic events was performed previously to the inversion. To achieve this, we used the LOCIN algorithm (Potin, 2016) in a gridded parallelepiped box constituted by cubes of 1 km length.

The Tikhonov problem to be solved in the inverse process for the travel time tomography consists of searching the minimum of a cost function over a regularization space where $C_d^{-1/2}$ and $C_m^{-1/2}$ represent the square root of the inverse of the prior covariance operator for the data **d** and model **m** vectors, respectively:

$$\left\| C_d^{-1/2}\left(d^{obs} - g(\boldsymbol{m}) \right) \right\|_D^2 + \left\| C_m^{-1/2}(\boldsymbol{m} - \boldsymbol{m}_{prior}) \right\|_M^2 \qquad (5)$$

The numerical representation of this equation is denoted as a quasi-Newton formulation implying the resolution of a linear system in the model space M at each iteration, where G_k is the derivative operator of g at a model parameter **m** in a fixed point k and G_k^* denotes their adjoint for the usual scalar products in D and M.

$$m_{k+1} - m_k = -(C_m^{-1} + G_k^* C_d^{-1} G_k)^{-1} \left(G_k^* C_d^{-1}(g(m_k) - d_{obs}) + C_m^{-1}(m_k - m_{prior}) \right) \,(6)$$

The Eq. (6) was solved using the INSIGHT computer code package, which uses the LSQR algorithm (Paige and Saunders, 1982) according to Monteiller et al., (2005). This tomography code was implemented in a gridded parallelepiped box with a cell size of 5 km in the horizontal direction and 2 km in the vertical direction. The code rewrites each iteration according to:

$$m_{k+1} - m_k = (A_k^* A_k)^{-1} A_k^* v_k \qquad (7)$$

8

Where:

$$A_k = \begin{bmatrix} C_d^{-1/2} G_k \\ Cor^{-1/2}\Sigma^{-1} \end{bmatrix} \qquad v_k = \begin{bmatrix} C_d^{-1/2}(g(m_k) - d_{obs}) \\ Cor^{-1/2}\Sigma^{-1}(m_k - m_{prior}) \end{bmatrix} \qquad (8)$$

The influence of both the damping and smoothing parameters was evaluated through L-curves graphics (Hansen, 1992) to obtain a realistic model. This allowed us to define the values of damping parameters ($\xi_0 = 9$ km, $\lambda = 0.5$) and the smoothing parameters ($\xi_V = 20$ km, $\xi_H = 35$ km).

Finally, to delimit the volume outside which the resolution of the inversion is surely very poor we evaluate the restitution (or averaging) index for the v_P and v_P/v_S models. The restitution index is a measure of the uncertainty in the velocity models, which allow us to identify the region where the intersection of seismic rays is sufficiently dense. Their value ranges from 0 to 1 for zones with high and low uncertainties, respectively. To obtain reliable results, we analyze only those regions with values of restitution index >0.7. We depict those regions of high uncertainties (<0.7) as white-shaded zones in the tomographic images. Under our working scheme, the practical computation of the restitution index is equivalent to performing an iteration of the inverse process.

RESULTS AND DISCUSSION

The resulting tomographic images are expressed in terms of the P velocity in absolute values (v_P), relative values (Δv_P), and the v_P/v_P ratio in vertical sections as indicated by the segments in Figure 2. The AA' segment encompasses the Antisana and Sumaco Volcano, whereas four volcanoes are included in the BB' segment: Reventador, Pan de Azúcar, Yanaurco and Sumaco.

According to the $\Delta \upsilon_P$ (Figure 3), we can identify a considerable difference in the velocities among the AA' and BB' segments. From these anomalies, it is possible to infer cortical structures such as lithology changes or delimited formations (Koulakov, 2013).

In the vertical AA' cross-section of the $\Delta \upsilon_P$ model (Figure 3 top), the positive values (>10%) just below the Antisana volcano could be related to the Paleozoic and Mesozoic metamorphic belts (Loja lithotectonic division), whereas the negative values (<-10%) below ~20 km could be related to a section of the Northern Andean Sliver (Aspden and Litherland, 1992; Hall et al., 2017). The BB' segment (Figure 3 bottom) clearly shows the difference of the basement among the volcanoes over the Napo Uplift and the Cordillera Real (Antisana).

All the Napo Uplift volcanoes (Reventador, Pan de Azúcar, Yanaurco, and Sumaco) are located upon the Jurassic-Cretaceous sedimentary sequence (Barragan et al., 1998; Barragán and Baby, 2004) following the values around 0% above ~16 km. Despite this, below the Sumaco seems to be a slight positive change (>0%), represented as green colors, which could be related to a variation in the rocks petrophysical properties of the rest of Napo Uplift. Below 16 km in this BB' segment, the negative anomalies could be associated with the South American Precambrian craton (Aspden and Litherland, 1992; Balkwill et al., 1995).

The most profound velocity anomalies of the cross-sections can be seen in Figure 4 and Figure 5 from both the υ_P and υ_P/υ_S models. From the υ_P model, it is possible to identify the Moho depth according to the increase in the P wave velocity and regions of high velocity that could be associated with a denser or a more consolidated structure (Koulakov, 2013). Here we consider the 6.8 km/s iso-value line from the υ_P model to identify the division between crust

and mantle. Otherwise, liquid structures associated with elevated temperatures could be determined from high anomalies of the υ_P/υ_S model (Koulakov, 2013; Koulakov and Shapiro, 2014).

From Figure 4, we can observe that the majority of the seismic events in this region occur at shallow zones within the crust (<35 km), whereas only a few events have taken place at greater depth in a range of 35 km and 115 km (upper mantle). The seismicity in the western flank of Sumaco volcano could be related to the strike-slip Sumaco Fault, which has a west dip transpressive dextral behavior with a <1 mm/yr slip rate (Eguez et al., 2003). Otherwise, the seismicity in the eastern flank of the Antisana volcano could be related to the compressional stress among the Cordillera Real and the Napo Uplift.

From the υ_P model of the AA' segment (Figure 4 top), it is possible to recognize a thickening of the crust ranging from ~60 km below Antisana to ~40 km under Sumaco according to the 6.8 km/s iso-value line. The highest values of P velocity (>8.1 km/s), denoted by purple colors, are located below ~100 km in all the extension between the Sumaco and Antisana. This high-velocity anomaly represents a higher density structure. A significant zone with expected liquid rocks is also recognizable from the υ_P/υ_S model of the AA' cross-section (Figure 4 bottom), which could be denoted by values greater or equal than 1.8. This high-value anomaly region is located predominantly below the Sumaco volcano, although it extends slightly westward.

According to the υ_P and υ_P/υ_S models of the BB' segment (Figure 5), the majority of seismic events are cortical (above ~35 km) and concentrated just below the Reventador active volcano, whereas there are few events at a depth greater than 35 km. The seismic events south

of Sumaco could be also related to the Sumaco fault (Eguez et al., 2003). The υ_P model of the BB' cross-section (Figure 5 top) shows a relatively constant width of the crust of ~45-50 km, following the 6.8 km/s iso-contour line. This crust thickening, greater than the 35 km of the Oriente Basin, below the Eastern Subandean Belt, proves this cordillera's roots. This figure also shows the highest P velocity (>8.1 km/s) below the Pan de Azúcar, Yanaurco, and Sumaco volcanoes at a depth between 100 km to 160 km, which again could be related to a higher density structure. Values greater than 1.8 in the υ_P/υ_S model of the BB' segment (Figure 5 bottom) also suggests the presence of a hotter or more liquid material. This structure seems to be predominantly located under Pan de Azúcar, Yanaurco, and Sumaco volcanoes.

Our results suggest the presence of 1) a section of an anomalous slab (below ~100 km) with values >8.1 km/s according to the υ_P model and 2) a magmatic reservoir in the most upper part of the mantle just below the crust, which is identified according to the high values anomalies (>1.8) of the υ_P/υ_S model. These structures are depicted in Figure 6 as 3D objects in depth.

The magmatic reservoir is situated in the southern part of the Napo Uplift and is positioned predominantly below the Sumaco volcano and shared with the Pan de Azúcar and Yanaurco volcanoes. This magmatic chamber is located from 35 to 60 km in depth. The anomalous slab found here is limited or restricted below the Reventador volcano, whereas it extends eastward from Antisana to Sumaco volcano, slightly increasing the angle of inclination.

The large-ion lithophile elements to high-field strength metals relation define the LIL/HFS ratio. Given that Sumacos lavas show a small LIL/HFS ratio and high content of incompatible

elements (Barragan et al., 1998; Barragán and Baby, 2004), this suggests a small contribution of the subducted slab and small degrees of partial melting. Therefore, the magmatic reservoir below this volcano seems to be charged by a possible slab-trap door mechanism (Rosenbaum et al., 2019) in a hypothetical flat slab. We suggest that the alkaline Sumaco lavas are formed from a mantellic source, which possibly rises by poloidal and toroidal flows. This mantellic source could be related to a slab block detached from ancient flat-slab subduction and currently situated over the Nazca subducted plate. This flows later produces a preferential partial melting of a Jurassic metasomatized mantle (Chiaradia et al., 2014) to finally reach and store this material in the magmatic reservoir shown in Figure 6.

From the relocated hypocenter's arrangement after the tomographic inversion (Figure 4, Figure 5), it is possible to deduce that the Sumaco fault extends ~25 km in depth. This structure could allow the rapid ascent of magmatic material to a shallower reservoir where recharge occurs before an eruptive event, as expected by Garrison et al. (2018). This rapid ascent could also explain the minimal crust assimilation of Sumaco lavas shown by ^{87}Sr/ ^{86}Sr and ^{143}Nd/ ^{144}Nd isotopes ratios (Barragán and Baby, 2004; Garrison et al., 2018).

CONCLUSIONS

The study of the subduction-related volcanic arc system in Ecuador sheds new light on understanding the dynamic between the South America continental plate and the oceanic Nazca Plate. According to our results, the volcanoes main magmatic reservoir over the Napo Uplift is disconnected from the volcanoes on the Real Cordillera.

From our υ_P model results, we can deduce that there is a considerable change in the elastic properties of the medium for which the seismic waves travel faster. The highest values (>8.1 km/s) at depths greater than 100 km suggest an anomalous slab restricted below the Reventador volcano and extends eastward while slightly increasing their inclination angle, below Sucamo volcano. The υ_P model shows a thickening crust below the Eastern Subandean Belt related to the root of this young cordillera.

According to our υ_P/υ_S model, the magmatic reservoir is located in the southern part of the Napo Uplift. Despite the proximity of Reventador, Pan de Azúcar, Yanaurco, and Sumaco volcanoes, the main magmatic reservoir inferred here is located predominantly below Sumaco. The depth of this magmatic chamber ranges from ~35 km to ~60 km, just below the crust. The extinct Pan de Azúcar and Yanaurco volcanoes shared this magma chamber in a reduced way. The melted mantle anomaly seems less related to the Reventador volcano.

The seismicity in the study area is concentrated just below the Reventador active volcano. This high seismicity could be related to the material rise through a vanishing point, such as long-depth active faults.

Considering previous studies of the Sumaco volcano and the tomographic results presented here, we propose that the geochemical differentiation of the Sumaco lavas could be related to two processes below and above the magmatic reservoir. Below the magmatic chamber, the flat slab arrangement allows a trap door mechanism that leads the rise of mantle materials by poloidal and toroidal flows that produce a preferential partial melting of a metasomatized mantle during its ascent until reaching the magmatic reservoir. On the other hand, the process

above the magmatic chamber that could explain to some extent the differentiation of Sumaco

lavas is related to the rapid ascent of the magmatic material through a fault plane (Sumaco

fault) towards the surface.

REFERENCES

Araujo, S., Travel time tomography of the crust and the mantle beneath Ecuador from data of the national seismic network, *Doctoral Thesis, Grenoble Alpes*, 2016.

Aspden, J. A. and Litherland, M., The geology and Mesozoic collisional history of the Cordillera Real, Ecuador, *Tectonophysics*, 1992, vol. 205, no 1-3, pp. 187-204.

Baby, P., Bernal, C., Christophoul, F. and Valdez, A., Modelo estructural y ciclos tectono-sedimentarios de la Cuenca Oriente, *Convenio ORSTOM PETROPRODUCCIÓN, Informe no publicado*, 1998, pp. 4-70.

Balkwill, H. R., Rodrigue, G., Paredes, F. I. and Almeida, J. P., Northern part of Oriente Basin, Ecuador: reflection seismic expression of structures, *AAPG Special Volumes*, 1995, pp. 559-571.

Barberi, F., Coltelli, M., Ferrara, G., Innocenti, F., Navarro, J. M. and Santacroce, R., Plio-quaternary volcanism in Ecuador, *Geological Magazine*, 1988, vol. 125, no. 1, pp. 1-14.

Barragán, R. and Baby, P., Evolución magmática actual de la zona subandina: volcanes El Reventador y Sumaco, modelos geodinámicos preliminares, *In Baby, P., Rivadeneira, M., and Barragán, R. (Eds.), La Cuenca Oriente: Geología y petróleo, Institut français d'études andines*, 2004, pp. 183-201.

Barragan, R., Geist, D., Hall, M., Larson, P. and Kurz, M., Subduction controls on the compositions of lavas from the Ecuadorian Andes, *Earth and Planetary Science Letters*, 1998, vol. 154, no. 1, pp. 153-166.

Bes de Berc, S. Tectonique de chevauchement, surrection et incision fluviatile: exemple de la zone subandine équatorienne, Haut bassin amazonien, *Doctoral dissertation, Toulouse*, 2003.

Bourdon, E., Eissen, J. P., Gutscher, M. A., Monzier, M., Hall, M. L. and Cotten, J., Magmatic response to early aseismic ridge subduction: the Ecuadorian margin case (South America), *Earth and Planetary Science Letters*, 2003, vo. 205, no. 3-4, pp. 123-138.

Bryant, J. A., Yogodzinski, G. M., Hall, M. L., Lewicki, J. L. and Bailey, D. G., Geochemical constraints on the origin of volcanic rocks from the Andean Northern Volcanic Zone, Ecuador, *Journal of petrology*, 2006, vol. 47, no. 6, pp. 1147-1175.

Chiaradia, M., Barnes, J. D. and Cadet-Voisin, S., Chlorine stable isotope variations across the Quaternary volcanic arc of Ecuador, *Earth and Planetary Science Letters*, 2014, vol. 396, pp. 22-33.

Chiaradia, M., Müntener, O., Beate, B. and Fontignie, D., Adakite-like volcanism of Ecuador: lower crust magmatic evolution and recycling, *Contributions to Mineralogy and Petrology*, 2009, vol. 158, no. 5, pp. 563-588.

Dashwood, M. F. and Abbotts, I. L., Aspects of the petroleum geology of the Oriente Basin, Ecuador, *Geological Society, London, Special Publications*, 1990, vol. 50, no. 1, pp. 89-117.

Eguez, A., Alvarado, A., Yepes, H., Machette, M. N., Costa, C., Dart, R. L. and Bradley, L. A., Database and map of Quaternary faults and folds of Ecuador and its offshore regions, *US Geological Survey Open-File Report*, 2003, vol. 3, pp. 289.

Gailler, A., Charvis, P. and Flueh, E. R., Segmentation of the nazca and south american plates along the ecuador subduction zone from wide angle seismic profiles, *Earth and Planetary Science Letters*, 2007, vol. 260, no. 3, pp. 444-464.

Garcia-Aristizabal, A., Kumagai, H., Samaniego, P., Mothes, P., Yepes, H. and Monzier, M., Seismic, petrologic, and geodetic analyses of the 1999 domeforming eruption of Guagua Pichincha volcano, Ecuador, *Journal of Volcanology and Geothermal Research*, 2007, vol. 161, no. 4, pp. 333-351.

Garrison, J. M., Sims, K. W., Yogodzinski, G. M., Escobar, R. D., Scott, S., Mothes, P., Hall, M. L. and Ramon, P., Shallow-level differentiation of phonolitic lavas from Sumaco Volcano, Ecuador, *Contributions to Mineralogy and Petrology*, 2018, vol. 173, no. 1, pp. 1-19.

Hall, M. L., El volcanismo en el Ecuador, Ecuador: IPGH Sección Nacional del Ecuador, 1977.

Hall, M. L., Mothes, P. A., Samaniego, P., Militzer, A., Beate, B., Ramón, P. and Robin, C., Antisana volcano: a representative andesitic volcano of the eastern cordillera of Ecuador: petrography, chemistry, tephra and glacial stratigraphy, *Journal of South American Earth Sciences*, 2017, vol. 73, pp. 50-64.

Ham C. K. and Herrera L. J., Role of Sub-Andean Fault System in Tectonics of Eastern Peru and Ecuador, *AAPG Bulletin*, 1963, vol. 45, no. 3, pp. 409.

Hansen, P. C., Analysis of discrete ill-posed problems by means of the L-curve, *SIAM review*, 1992, vol. 34, no. 4, pp. 561-580.

Hidalgo, S., Gerbe, M. C., Martin, H., Samaniego, P. and Bourdon, E., Role of crustal and slab components in the Northern Volcanic Zone of the Andes (Ecuador) constrained by Sr–Nd–O isotopes, *Lithos*, 2012, vol. 132, no. 1., pp. 180-192.

Husen, S., Smith, R. B. and Waite, G. P., Evidence for gas and magmatic sources beneath the Yellowstone volcanic field from seismic tomographic imaging, *Journal of Volcanology and Geothermal Research*, 2004, vol. 131, no. 3, pp. 397-410.

Koulakov, I. and Shapiro, N., Seismic tomography of volcanoes, *Encyclopedia of Earthquake Engineering, Springer, Dordrecht*, 2015, pp. 3117-3134.

Koulakov, I., Studying deep sources of volcanism using multiscale seismic tomography, *Journal of volcanology and geothermal research*, 2013, vol. 257, pp. 205-226.

Laraque, A., Bernal, C., Bourrel, L., Darrozes, J., Christophoul, F., Armijos, E., Fraizy, P., Pombosa, R. and Guyot, J. L., Sediment budget of the Napo river, Amazon basin, Ecuador and Peru, *Hydrological Processes: An International Journal*, 2009, vol. 23, no. 25, pp. 3509-3524.

Lees, J. M., Johnson, J. B., Ruiz, M., Troncoso, L. and Welsh, M., Reventador Volcano 2005: Eruptive activity inferred from seismo-acoustic observation, *Journal of Volcanology and Geothermal Research*, 2008, vol. 176, no. 1, pp. 179-190.

Legrand, D., Baby, P., Bondoux, F., Dorbath, C., De Berc, S. B. and Rivadeneira, M., The 1999–2000 seismic experiment of Macas swarm (Ecuador) in relation with rift inversion in Subandean foothills, *Tectonophysics*, 2005, vol. 395, no. 1, pp. 67-80.

Li, C., y van der Hilst, R. D., Structure of the upper mantle and transition zone beneath southeast asia from traveltime tomography, *Journal of Geophysical Research: Solid Earth*, 2010, vol. 115, no. B7, pp. 1-19.

Lynner, C., Koch, C., Beck, S. L., et al., Upper-plate structure in Ecuador coincident with the subduction of the Carnegie Ridge and the southern extent of large mega-thrust earthquakes, *Geophysical Journal International*, 2020, vol. 220, no. 3, pp. 1965-1977.

McNamara, D. E., Walter, W. R., Owens, T. J. and Ammon, C. J., Upper mantle velocity structure beneath the Tibetan Plateau from Pn travel time tomography, *Journal of Geophysical Research: Solid Earth*, 1997, vol. 102, no. B1, pp. 493-505.

Molina, I., Kumagai, H., Le Pennec, J.-L. and Hall, M., Three-dimensional P-wave velocity structure of Tungurahua Volcano, Ecuador, *Journal of Volcanology and Geothermal Research*, 2005, vol. 147, no. 1, pp. 144 - 156.

Monteiller, V., Got, J. L., Virieux, J. and Okubo, P., An efficient algorithm for double-difference tomography and location in heterogeneous media, with an application to the Kilauea volcano, *Journal of Geophysical Research: Solid Earth*, 2005, vol. 110, no B12, pp. 1-22.

Nolet, G., A breviary of seismic tomography: Imaging the interior of the earth and sun, Cambridge: Cambridge University Press, 2008.

Paige, C. and Saunders, M., An algorithm for sparse linear equations and sparse least squares: ACM Transactions in Mathematical Software. 1982.

Paulatto, M., Annen, C., Henstock, T. J., Kiddle, E., Minshull, T. A., Sparks, R. S. J. and Voight, B., Magma chamber properties from integrated seismic tomography and thermal modeling at Montserrat, *Geochemistry, Geophysics, Geosystems*, 2012, vol. 13, no. 1, pp. 1-18.

Potin, B., Les Alpes occidentales: tomographie, localisation de séismes et topographie du Moho, *Doctoral Thesis, Grenoble Alpes}*, 2016.

Prevott, R., Chatelain, J.-L., Guillier, B. and Yepes, H., Tomographie des andes équatoriennes: évidence d'une continuité des andes centrales, *Comptes Rendus de l'Academie des Sciences-Serie IIa-Sciences de la Terre et des Planetes*, 1996, vol. 323, no. 10, pp. 833-840.

Rosenbaum, G., Sandiford, M., Caulfield, J. and Garrison, J. M., A trapdoor mechanism for slab tearing and melt generation in the northern Andes, *Geology*, 2019, vol. 47, no 1, pp. 23-26.

Rowan, L. R. and Clayton, R. W., The three-dimensional structure of Kilauea Volcano, Hawaii, from travel time tomography, *Journal of Geophysical Research: Solid Earth*, 1993, vol. 98, no. B3, pp. 4355-4375.

Ruiz, G. M. H., Exhumation of the northern Sub-Andean Zone of Ecuador and its source regions: a combined thermochronological and heavy mineral approach, *Doctoral dissertation, ETH Zurich*, 2002.

Salgado, J. A., Estudio de los depósitos volcánicos desde el Pleistoceno superior del volcán Sumaco, provincias de Napo y Orellana, *Bachelor's thesis, Quito*, 2019.

Sekiguchi, S., A new configuration and an aseismic slab of the descending Philippine Sea plate revealed by seismic tomography, *Tectonophysics*, 2001, vol. 341, no. 1, pp. 19-32.

Siebert, L., Simkin, T. and Kimberly, P., Volcanoes of the World, California: University of California Press, 2011.

Spakman, W., van der Lee, S., and van der Hilst, R., Travel-time tomography of the European-Mediterranean mantle down to 1400 km, *Physics of the Earth and Planetary Interiors*, 1993, vol. 79, no. 1, pp. 3-74.

Tarantola, A. and Valette, B., Generalized nonlinear inverse problems solved using the least squares criterion, *Reviews of Geophysics*, 1982, vol. 20, no 2, p. 219-232.

Thouvenot, F. and Fréchet, J., Seismicity along the northwestern edge of the Adria microplate. *In The Adria Microplate: GPS Geodesy, Tectonics and Hazards*, Dordrecht: Springer, 2006. p. 335-349.

Volynets, A. O., Churikova, T. G., Wörner, G., Gordeychik, B. N. and Layer, P., Mafic Late Miocene–Quaternary volcanic rocks in the Kamchatka back arc region: implications for subduction geometry and slab history at the Pacific–Aleutian junction, *Contributions to Mineralogy and Petrology*, 2010, vol. 159, no. 5, 659-687.

Wadati, K. and Oki, S., On the travel time of earthquake waves (Part II), *Journal of the Meteorological Society of Japan Ser. II*, 1933, vol. 11, no. 1, pp. 14-28.

Zhao, D., Multiscale Seismic Tomography, Japan: Springer Japan, 2015.

Zhou, H.-W. and Clayton, R., P and S wave travel time inversions for subducting slab under the island arcs of the northwest Pacific, J. *Geophys*, 1990, vol. 95, no. B5, pp. 6829-6851.
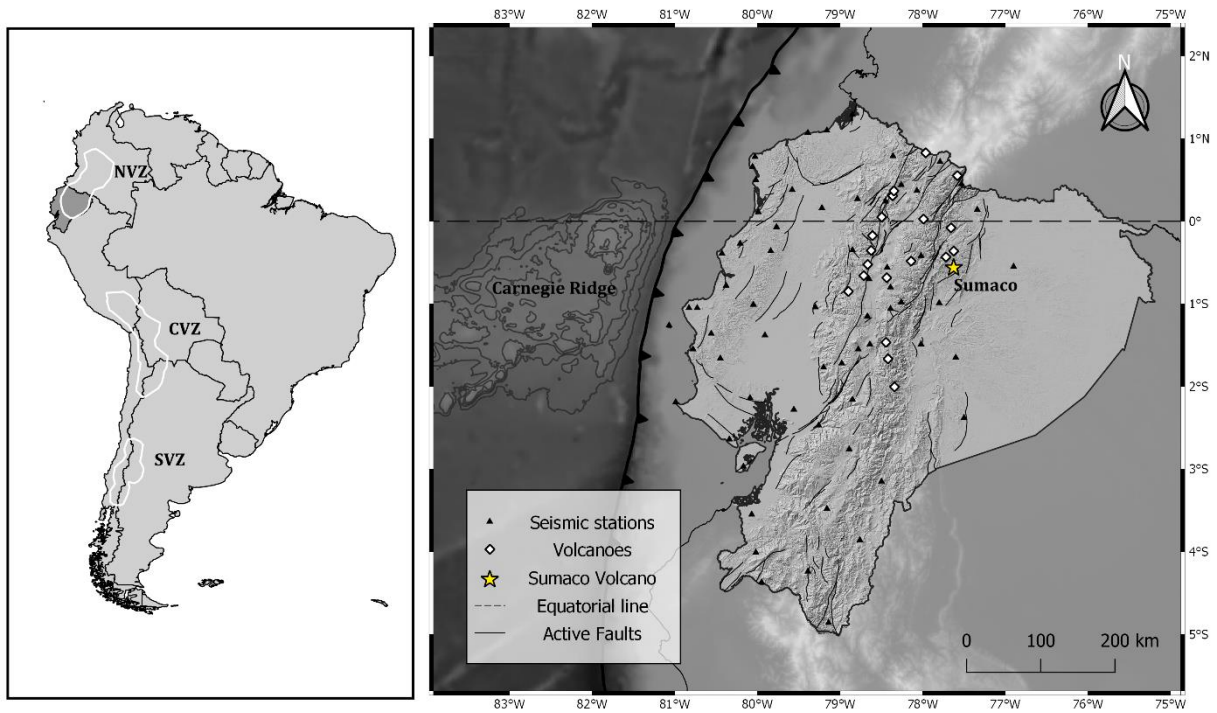
Figure 1: Regional location map and simplified tectonic map of Ecuador. Black triangles represent the seismic stations, while active Quaternary volcanoes over the Andes are represented with white dots. The Sumaco volcano position is the yellow star. The major active faults in Ecuador are depicted as black lines.
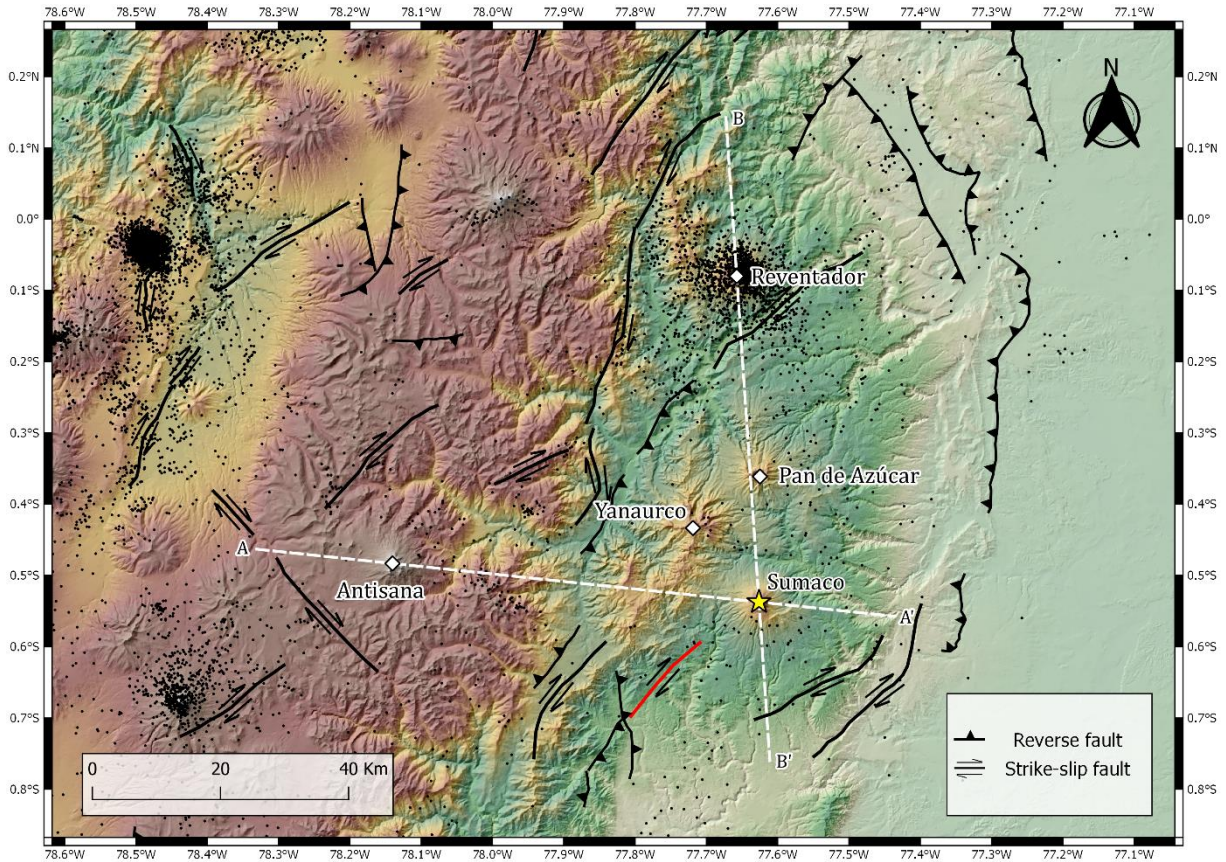
Figure 2: Digital elevation model of the study area. The figure shows the major active faults (black lines) and the division between the Cordillera Real (brown) and the Napo Uplift (dark green), as well as the seismicity associated (black dots) to the volcanoes in this zone. The Sumaco Fault is depicted as a red line. The AA' cross section is centered in -77.883 W, -0.510 S with an azimuth of S 84° E, and the BB' cross section is centered in -77.642 W, -0.309 S with an azimuth of S 4° E.
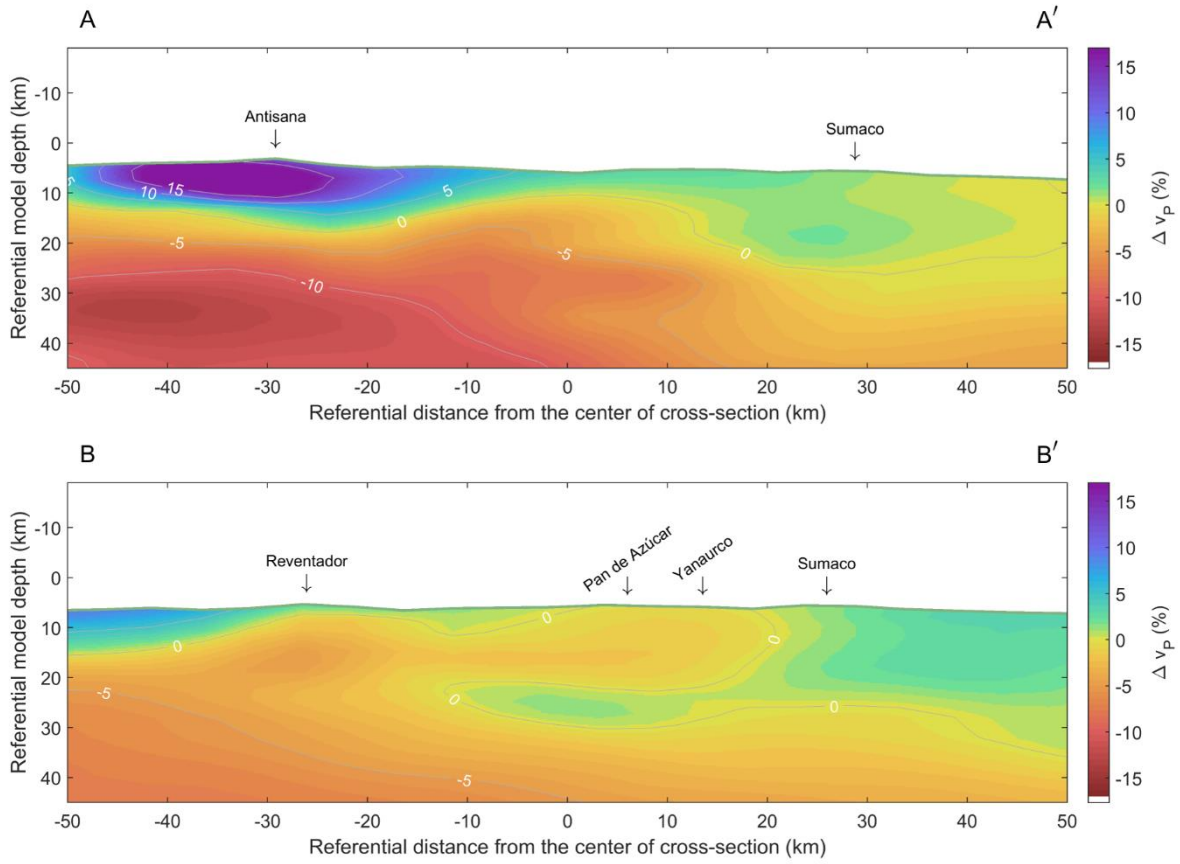
Figure 3: Cross-sections of the Δv_P model for the AA' and BB' sections. The axis units are in km. Main geological formations and contacts are visible by the Δv_P contrast.
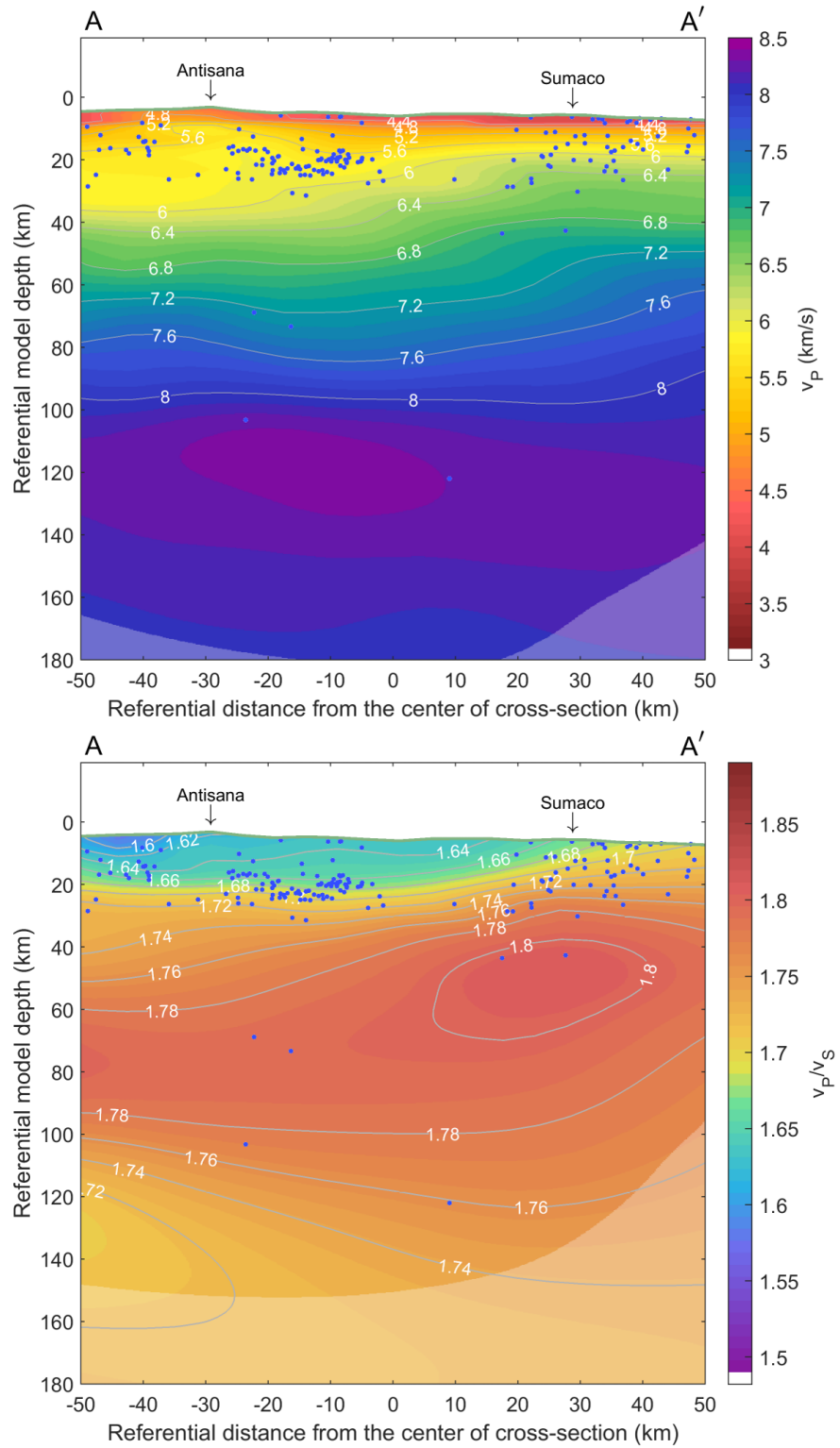
Figure 4: Cross-sections of the v_P and v_P/v_S velocity models for the AA' segment. The hypocenters of the seismic events after the inversion process are depicted as blue dots. These

events are comprised among 10 km away on the cross-sections side. The white-shaded zones

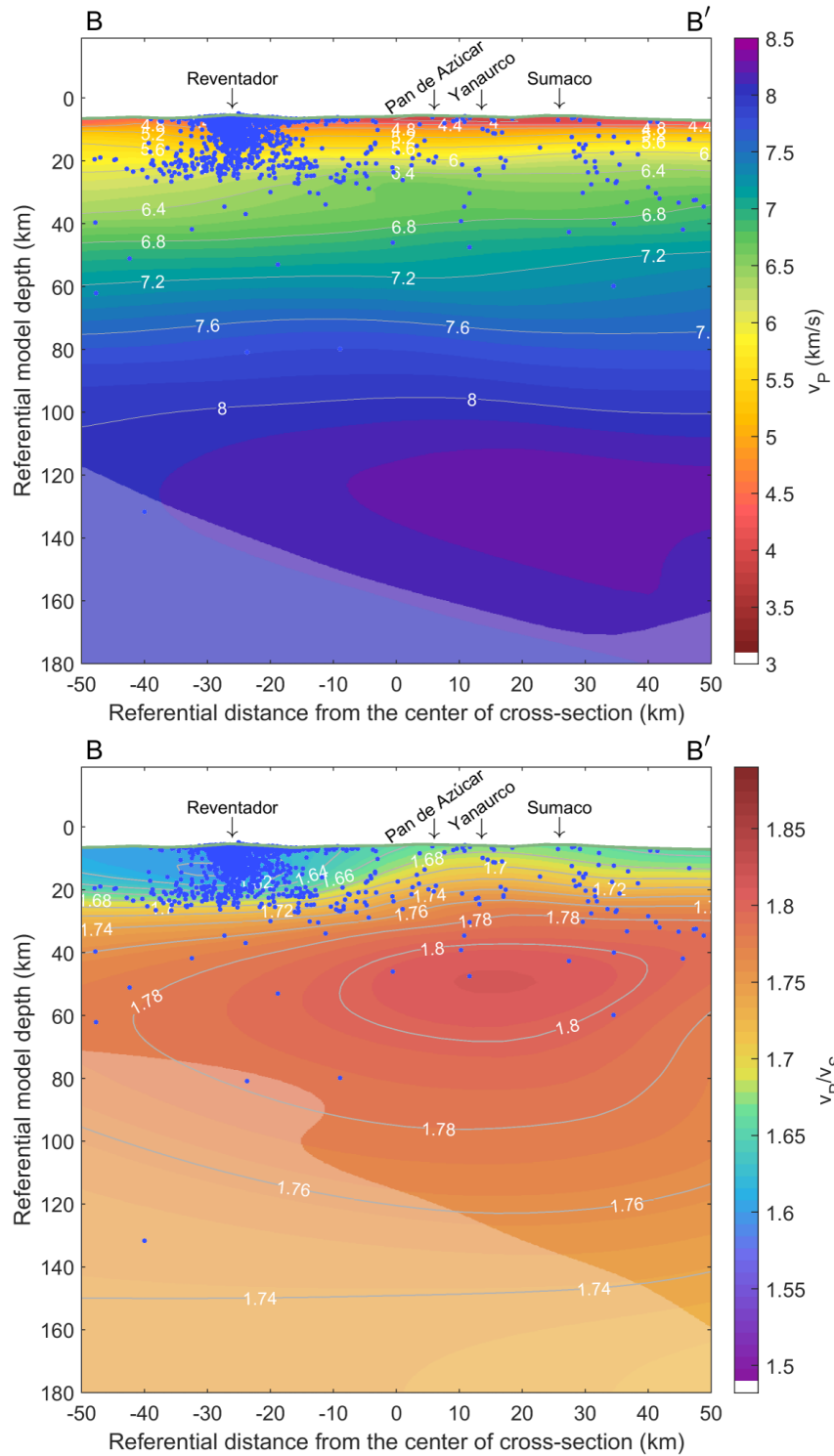denote the regions with a low-restitution index (<0.7). The axis units are in km.

Figure 5: Cross-sections of the v_P and v_P/v_S velocity models for the BB′ segment. The hypocenters of the seismic events after the inversion process are depicted as blue dots. These

events are comprised among 10 km away on the cross-sections side. The white-shaded zones denote the regions with a low-restitution index (<0.7). The axis units are in km.
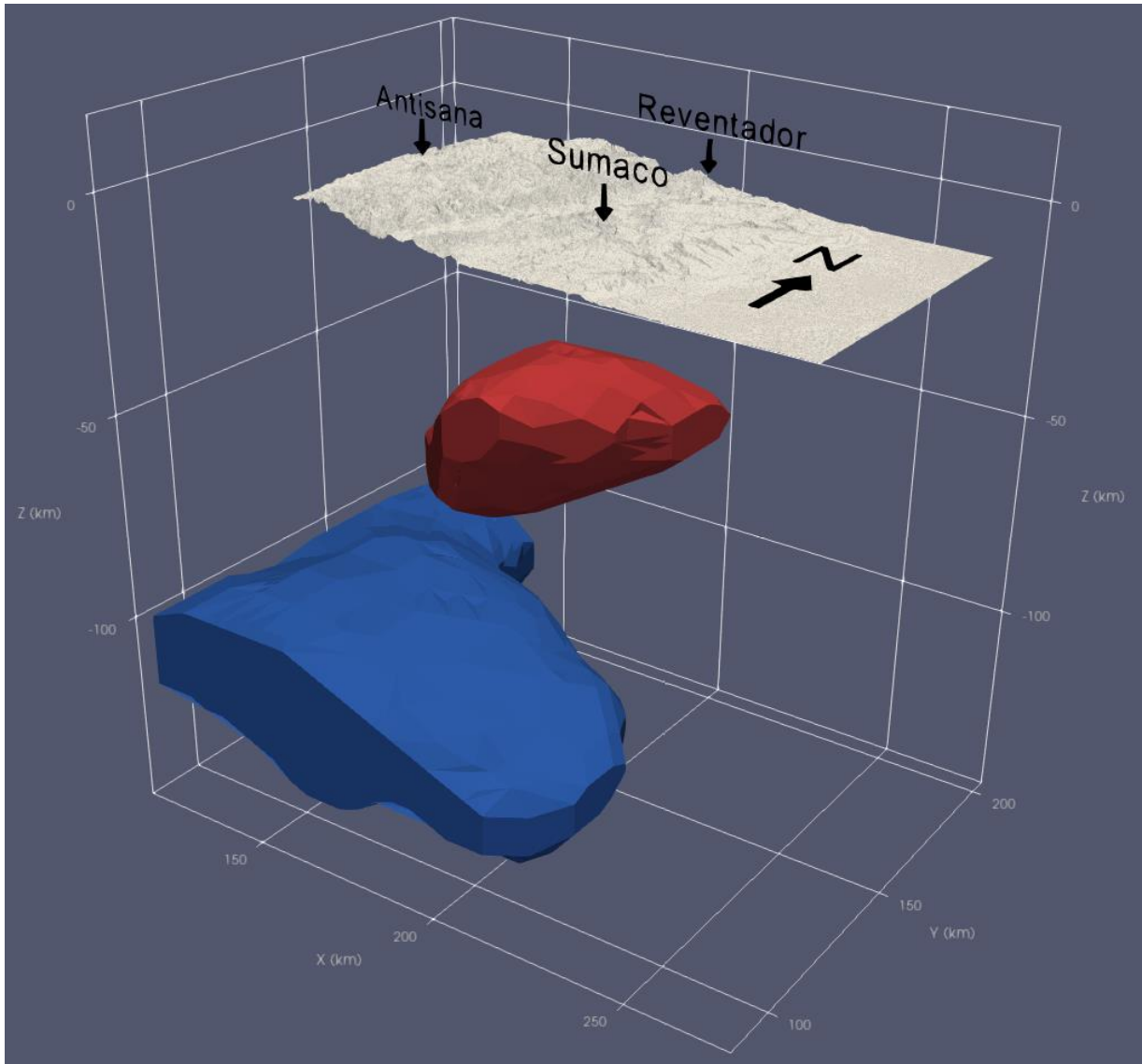

Figure 6: Three-dimensional sketch of the identified structures in depth. The figure shows an anomalous slab (blue) from the v_P model and the main magmatic reservoir (red) from the v_P/v_S model. The reservoir is located predominantly below Sumaco volcano although is also shared between Pan de Azúcar and Yanaurco volcanoes. The z-axis represents the depth in km

from the surface, while the x-axis and y-axis represent the referential horizontal distances in

km in the area of interest.